

# CONTRIBUTION TO NEUTRON FLUENCE AND NEUTRON ABSORBED DOSE FROM DOUBLE SCATTERING PROTON THERAPY SYSTEM COMPONENTS

A. PÉREZ-ANDÚJAR\* *University of Wisconsin School of Medicine and Public Health, 750 Highland Avenue 4111 HSLC, Madison, Wisconsin 53705-2221*

W. D. NEWHAUSER *The University of Texas M. D. Anderson Cancer Center Department of Radiation Physics, Unit 94, 1515 Holcombe Boulevard Houston, Texas 77030*

P. M. DeLUCA, Jr. *University of Wisconsin, School of Medicine and Public Health 750 Highland Avenue, 4111 HSLC, Madison, Wisconsin 53705-2221*

Received April 30, 2008

Accepted for Publication May 16, 2009

*Proton therapy offers low integral dose and good tumor conformality in many deep-seated tumors. However, secondary particles generated during proton therapy, such as neutrons, are a concern, especially for passive scattering systems. In this type of system, the proton beam interacts with several components of the treatment nozzle that lie along the delivery path and can produce secondary neutrons. Neutron production along the beam's central axis in a double scattering passive system was examined using Monte Carlo simulations. Neutron fluence and energy distribution were determined downstream of the nozzle's major components at different radial distances from the central axis. In addition, the neutron*

*absorbed dose per primary proton around the nozzle was investigated. Neutron fluence was highest immediately downstream of the range modulator wheel (RMW) but decreased as distance from the RMW increased. The nozzle's final collimator and snout also contributed to the production of high-energy neutrons. In fact, for the smallest treatment volume simulated, the neutron absorbed dose per proton at isocenter increased by a factor of 20 due to the snout presence when compared with a nozzle without a snout. The presented results can be used to design more effective local shielding components inside the treatment nozzle as well as to better understand the treatment room shielding requirements.*

## I. INTRODUCTION

Protons were first proposed for radiotherapy in 1946 (Refs. 1 and 2). The principal advantage of protons is the physical dose distribution compared to conventional radiotherapy as well as the rapid dose falloff at the end of the proton range and a sharp lateral penumbra. These

features lower the integral dose and the dose to organs at risk.<sup>3,4</sup>

Two principal proton delivery systems are currently used: active scanning systems and passive scattering systems. In passive scattering systems, the proton beam interacts with energy degraders and scattering foils in the treatment nozzle to create a spread-out Bragg peak (SOBP). The energy degraders modulate the penetrability of the beam, and the scattering foils spread the beam laterally.<sup>5</sup> Collimators and boluses can also be used to

\*E-mail: perezandujar@wisc.edu

shape the beam further. In contrast, active scanning systems have fewer beam-shaping devices in the treatment nozzle because beam spots are magnetically scanned throughout the treatment volume. The beam's interaction with shaping devices will produce secondary particles such as neutrons. In fact, some studies have presented neutron dose differences of one order of magnitude between active and passive systems, suggesting that passive systems produce much higher neutron doses than active systems.<sup>6,7</sup> However, more recent studies have shown that the difference in neutron production between the two systems is smaller than previously reported.<sup>8-10</sup>

In this study, we provide a progress report on estimates of the neutron production in a double scattering system. This work expands on earlier studies by using actual proton fluence weights for a typical SOBPs to better understand neutron production within the treatment nozzle.<sup>11</sup> In this system, the range modulation wheel (RMW) is made of a combination of high-*Z* and low-*Z* materials, which simultaneously modulate the beam's range and spread the beam laterally. The second scatterer, which further spreads the beam laterally, is also made of low- and high-*Z* materials.<sup>12,13</sup> The overall purpose of this work was to determine the neutron contribution from each component in the nozzle that shapes the proton beam. To accomplish this, we used Monte Carlo simulations to model the passive scattering beam nozzle as well as the interactions of the proton beam that lead to the production of secondary neutrons.

## II. METHODS AND MATERIALS

### II.A. Monte Carlo Model

The treatment nozzle's major components were modeled following the design of the double scattering passive system used at the Proton Therapy Center at M. D. Anderson Cancer Center.<sup>14,15</sup> The model includes a nonproprietary RMW similar, but not identical, to that of the Hitachi IBA system.<sup>14</sup> It also includes a secondary scatterer, collimators, and snout. No beam-monitoring components nor additional range-modulation devices were included. Simulations were performed using the Monte Carlo code MCNPX developed by Los Alamos National Laboratory, which has been extensively used in proton therapy applications.<sup>16-22</sup> In the simulations, a proton beam was transported through the nozzle and interacted with the nozzle's components before being completely stopped in a water phantom. As part of the beam interactions with the nozzle components, neutrons were produced and were also transported. For neutrons with energies ranging from thermal to 150 MeV, nuclear interaction probabilities were obtained from the Evaluated Nuclear Data File (ENDF) library; for neutrons with energies above 150 MeV, cross sections were calculated

using physics nuclear interaction models (specifically, the Bertini intranuclear cascade model).<sup>23,24</sup>

### II.B. Geometry

In this work, two geometries of the same treatment nozzle were simulated (see Figs. 1 and 2). First, a 200-MeV proton beam traveled through the treatment nozzle, interacting with the RMW, second scatterer, and a collimating system before stopping in a water phantom (Fig. 1). The cylindrical phantom's face was at isocenter and had a diameter and thickness of 300 mm. The RMW was made of a lamination of high- and low-*Z* materials, and the second scatterer was made of low- and high-*Z* materials. The high-*Z* material was lead, and the low-*Z* material was polymethyl methacrylate (PMMA). The characteristics of the RMW and double scatterer used in these simulations have been described elsewhere.<sup>11</sup> The collimators were made of copper and, for clarity, are classified as primary, secondary, tertiary, and final collimators. The primary collimator had a 70-mm thickness, the secondary, 120 mm, and the tertiary and final collimators were both 60 mm thick. The snout, which is another component of the collimating system, was located at the treatment nozzle's end and had a variable size aperture made of copper. Further nozzle dimensions are presented in Fig. 2.

The snout's square aperture along with the thickness of the RMW were varied to irradiate three treatment volumes in the water phantom:  $50 \times 50 \times 50 \text{ mm}^3$ ,  $100 \times 100 \times 100 \text{ mm}^3$ , and  $150 \times 150 \times 150 \text{ mm}^3$ . By varying the RMW thicknesses, as well as the beam weights for each thickness, a uniform SOBPs was obtained. The same secondary scatterer was used for all the treatment volumes simulated. To score the neutron fluence as a function of radial distance from the beam's central axis, several concentric cylinders with diameters ranging from 5 to 200 mm and a thickness of 1 mm were used as detecting volumes. These were placed at four locations along the beam's central axis: 200 mm downstream of the RMW junction between the high- and low-*Z* materials, 100 mm downstream of the second scatterer material junction, as well as 100 mm upstream and downstream of the snout. The detecting volumes were simulated as vacuum since their only purpose was to score the neutrons crossing that region.

For the second set of simulations, the water phantom and the detecting surfaces along the nozzle's central axis were removed (Fig. 2). Instead, cylindrical surfaces of 125 mm in radius and 1 mm thick were placed at different angles and at 3.06 m with respect to the RMW. These surfaces were used to determine the variation in neutron absorbed dose per proton around the nozzle due to the interaction of the beam with the individual beam-shaping components. The simulations were first run for the 200-MeV proton beam interacting only with the RMW; subsequently, the remaining nozzle components were added one at a time.

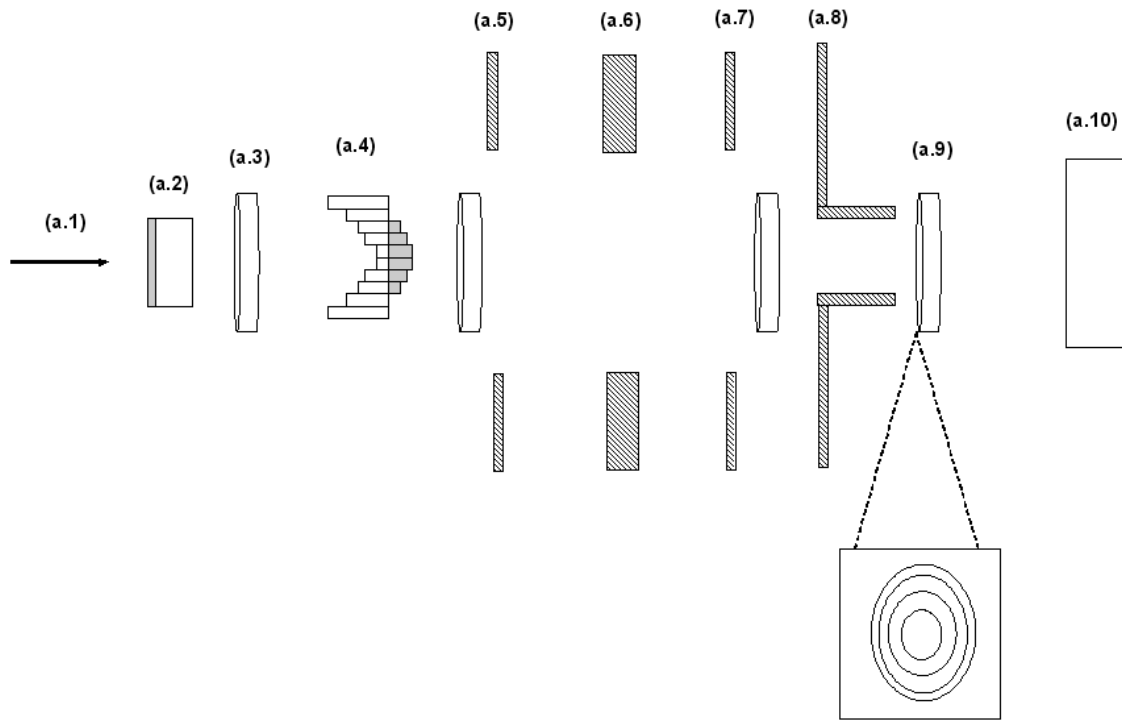


Fig. 1. Treatment nozzle geometry used in the first set of simulations using the MCNPX code. (a.1) Monoenergetic 200-MeV proton beam; (a.2) RMW; (a.3) detecting volumes; (a.4) second scatterer; (a.5) primary, (a.6) secondary, and (a.7) tertiary collimators; (a.8) final collimator and variable aperture; (a.9) zoom-in window showing the concentric cylinders that form the detecting volumes; and (a.10) water phantom. Note: figure not shown to scale.

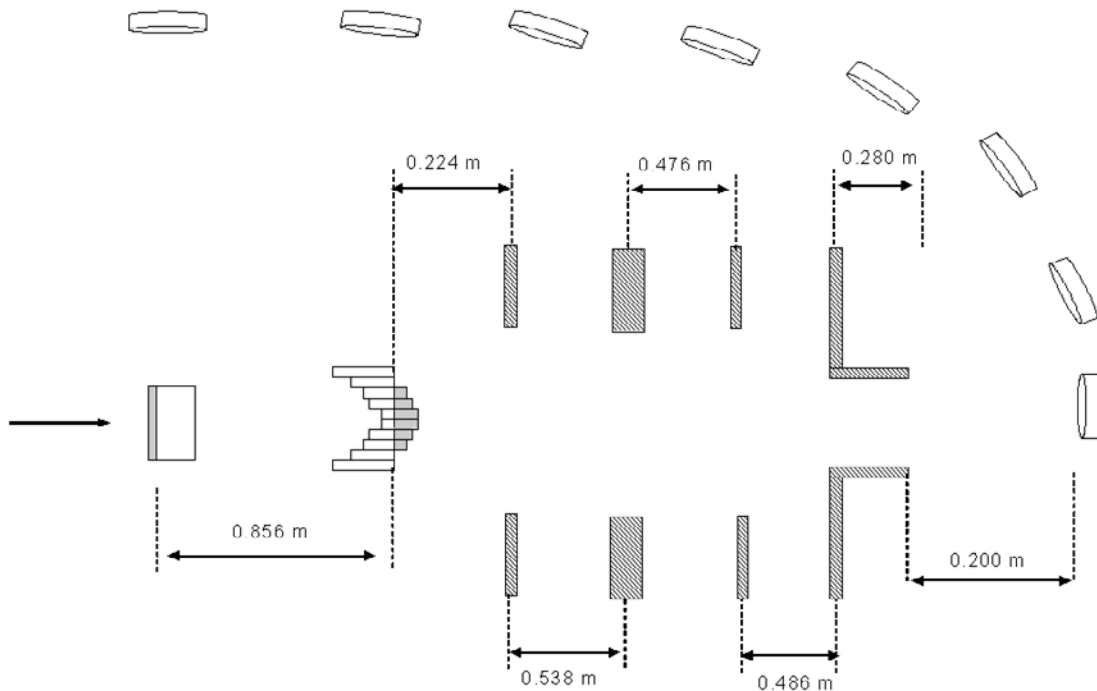


Fig. 2. Geometry used for the neutron dose determination simulations. Treatment nozzle distances between components were the same for both sets of simulations. Distances between collimators are given from the middle of each one. Note: figure not shown to scale.

### III. RESULTS AND DISCUSSION

#### III.A. Neutron Fluence

Figures 3a, 3b, and 3c show the neutron fluence as a function of the radial distance for each one of the four positions studied. Neglecting the neutrons scored at the volume just upstream of the snout, whose behavior will be explained later, the highest neutron fluence was found downstream of the RMW. After the RMW, the neutron fluence diminished as distance from the RMW increased. On average, the neutron fluence was ~30% higher for the largest treatment volume ( $150 \times 150 \times 150 \text{ mm}^3$ ), for which the largest total amount of high- and low-Z mate-

rial was used, than for the smallest one at the location immediately downstream of the RMW. Figure 4a shows neutron energy spectra at 20- to 25-mm radial distance from the central axis just downstream of the RMW and the snout for the smallest and largest treatment volumes. The maximum fluence occurred just downstream of the RMW and is the largest for the largest treatment volume, although at higher energies above 175 MeV, it is close to that of the smallest treatment volume. This behavior was seen up to ~100 mm from the beam's central axis; beyond this distance, the neutron fluence and energy decreased sharply (Fig. 4b). On the other hand, after the snout, the fluence of energetic neutrons was slightly higher than before as the radial distance increases (Fig. 4b). The

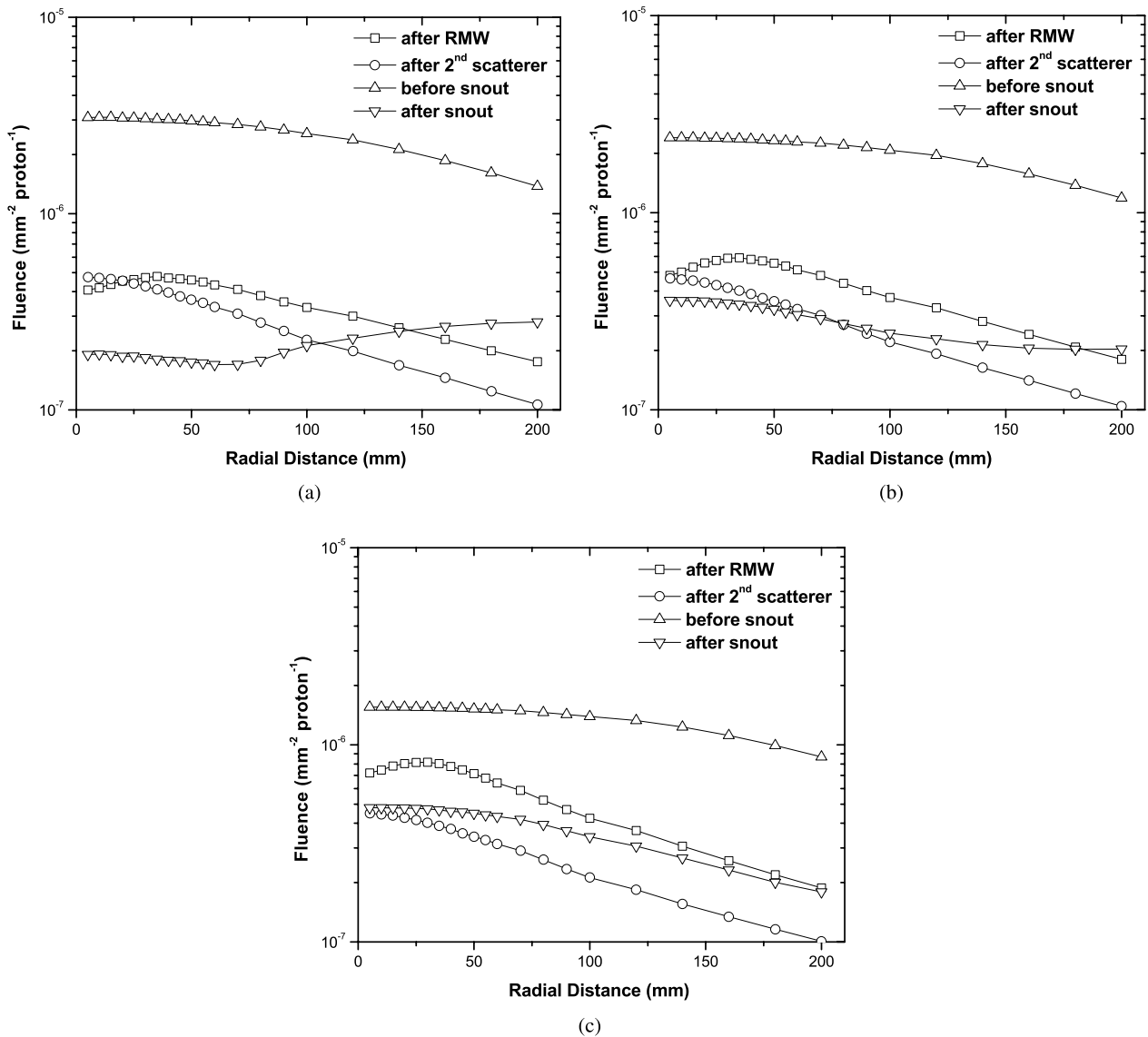


Fig. 3. Total neutron fluence as a function of radial distance from the beam's central axis for the three treatment volumes studied: (a)  $50 \times 50 \times 50 \text{ mm}^3$ , (b)  $100 \times 100 \times 100 \text{ mm}^3$ , and (c)  $150 \times 150 \times 150 \text{ mm}^3$ .

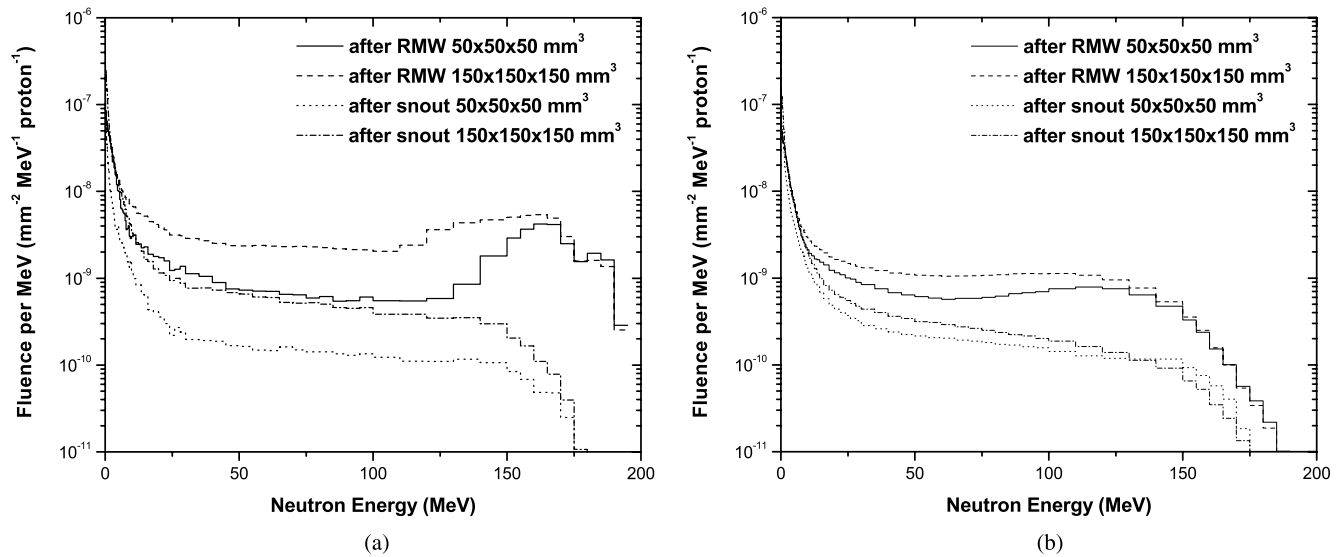


Fig. 4. Neutron energy spectra, as a function of neutron energy: (a) at a radial distance from 20 to 25 mm from the beam’s central axis downstream of the RMW and snout and (b) at a radial distance from 120 to 140 mm at the same locations.

reason for this behavior is that high-energy protons were collimated by the snout, generating high-energy neutrons.

A large neutron fluence was observed just upstream of the snout. This is attributed to backscatter effects. To determine if this behavior is in fact because of backscatter, the copper’s density at the snout was decreased by 20, 50, and 70%. This was done only for the smallest treatment volume for which the largest amount of collimating material is present in the beamline. As the density was

decreased, the neutron fluence upstream of the snout decreased dramatically (Fig. 5a). On the other hand, the opposite behavior was seen downstream of the snout, suggesting that although the snout was a source of neutrons, it also shielded some of them (Fig. 5b). Also, an increase in fluence was observed after a radial distance of 60 mm for the case where the collimator had its full density. This behavior could be attributed to scattered neutrons from the final collimator and snout. Note that

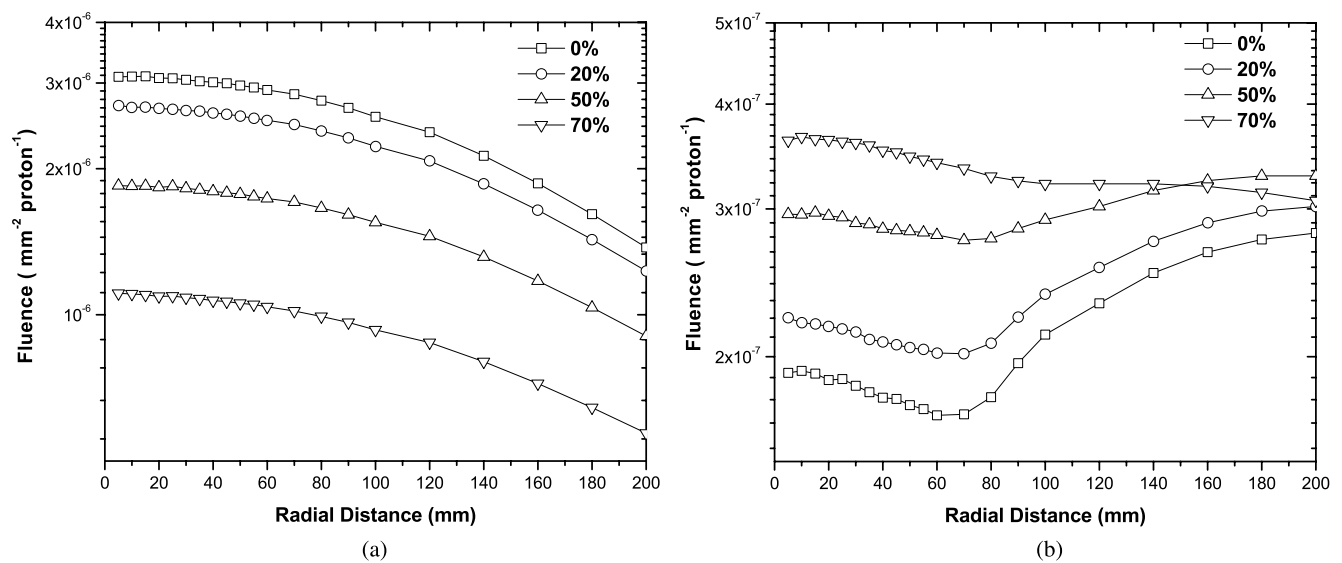


Fig. 5. Neutron fluence dependency on the snout’s copper density (a) just upstream and (b) downstream of the snout. Percentages represent the reduction in copper density.

the water phantom is present in all of these simulations, so there will be some contribution to the neutron fluence by this.

### III.B. Neutron Absorbed Dose per Proton

Figures 6a and 6b show the neutron absorbed dose per proton around the treatment nozzle for the smallest and largest treatment volume configurations used for the first set of simulations. These simulations did not have the water phantom present because their objective was to calculate the contribution to the neutron fluence only by the nozzle components. The neutron absorbed dose was calculated by multiplying the neutron fluence at each surface by the appropriate kerma coefficients obtained from ICRU Report 63 (Ref. 25). The neutron absorbed dose is due only to the interaction of the proton beam with the nozzle shaping components. It was observed that the neutron dose increases for all angles when the snout is present in the geometry. The dose increases by a factor of 20 at isocenter for the smallest treatment volume and by  $\sim 10$  for the largest one. A slightly higher factor was found at 5 deg. This was  $\sim 30$  and 20 for the smallest and the largest fields, respectively. Above 5 deg, the neutron absorbed dose starts to decrease, although it is still higher at all angles than in simulations where the snout was not present. The higher neutron absorbed dose could be in part due to the proximity of the detecting surfaces to the snout. In addition, this is the highest for

the smallest treatment volume, because the largest amount of collimating material in the snout is present in the beam path for this configuration. Overall, the detecting cylinders are closer to the snout than to the RMW and secondary scatterer.

### IV. CONCLUSION

Using Monte Carlo simulations, we found that the RMW was the highest contributor to neutron production within the treatment nozzle. This result was expected, because the RMW is the nozzle component that has the largest amount of material in the proton beam path. These results may vary from institution to institution because this depends on the type of material used for the RMW. Specifically, the RMW simulated had simultaneously high- and low-Z material, while for some institutions, the RMW is made only from low-Z material and the high-Z material is placed separately along the nozzle. We also found that the neutron fluence decreased as a function of distance from the RMW. The maximum fluence of high-energy neutrons was found at radial distances closer to the beam's central axis, indicating that neutron production is forward directed. Thus, as distance from the beam's central axis increased, the neutron fluence decreased. The snout and collimator also contributed to the neutron fluence. In fact, in the simulations discussed in this paper, the snout

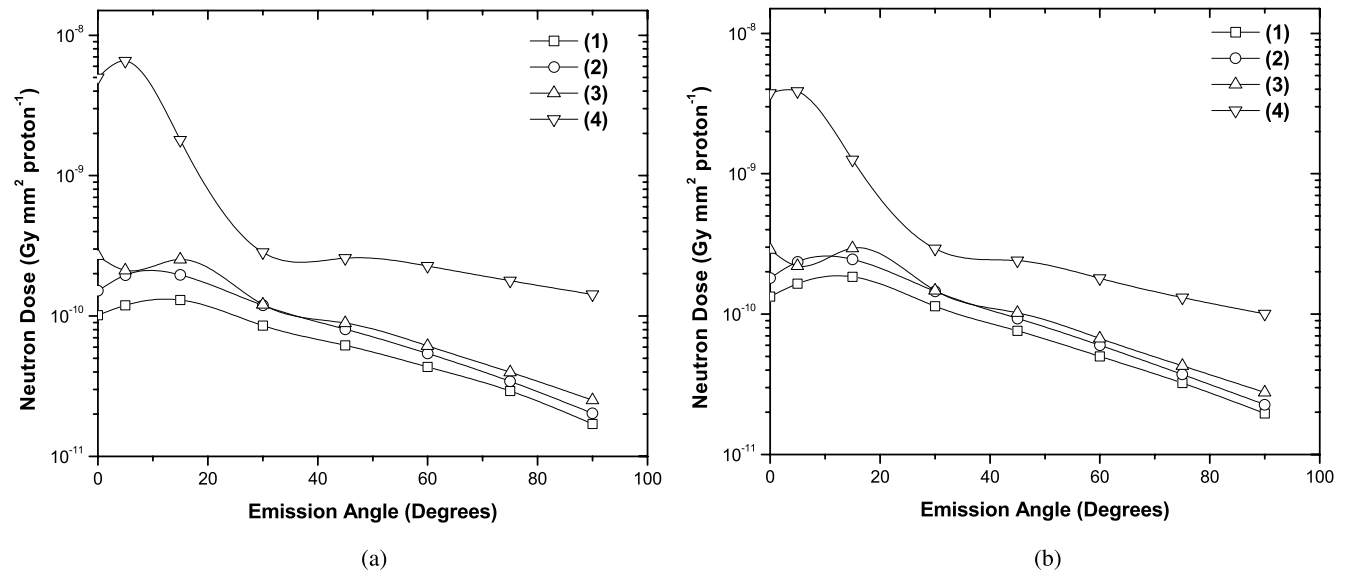


Fig. 6. Neutron absorbed dose around the treatment nozzle for (a) the smallest treatment volume,  $50 \times 50 \times 50 \text{ mm}^3$ , and for (b) the largest one,  $150 \times 150 \times 150 \text{ mm}^3$ . In both figures, (1) represents the case when only the RMW is present in the nozzle and the remaining components were set to vacuum, (2) when the RMW and secondary scatterer are present, (3) for the RMW, second scatterer, and primary, secondary, and tertiary collimators, and (4) is the complete nozzle with the addition of the final collimator and snout. The neutron absorbed dose is normalized to the number of source protons and the distance squared from the RMW junction and the detecting volume, 3.06 m.

dominates the neutron absorbed dose per proton for all angles near isocenter. Our results indicate that the RMW is the primary source of neutrons inside the treatment nozzle, while the snout dominates the neutron dose at isocenter and those locations closer to it. Therefore, it might be possible to decrease the neutron production in the nozzle as well as the required room shielding by adding the appropriate combination of shielding in the treatment nozzle.

### ACKNOWLEDGMENTS

This work was supported in part by the National Science Foundation (NSF) and the University of Wisconsin-funded Grid Laboratory (GLOW) computer cluster (NSF award 0320708). Funding was provided by the National Institute of Health Ruth L. Kirschstein National Research Service Award Individual Predoctoral Fellowship Program (award F31 CA119943-03) and by Northern Illinois University through a subcontract of the U.S. Department of Defense (contract W81XWH-08-1-0205) (W. D. Newhauser).

### REFERENCES

1. R. R. WILSON, "Radiological Use of Fast Protons," *Radiology*, **47**, 487 (1946).
2. D. W. MILLER, "A Review of Proton Beam Radiation Therapy," *Med. Phys.*, **22**, 1943 (1995).
3. B. GLIMELIUS, U. ISACSSON, E. BLOMQUIST, E. GRUSELL, B. JUNG, and A. MONTELIUS, "Potential Gains Using High-Energy Protons for Therapy of Malignant Tumors," *Acta Oncol.*, **38**, 2, 137 (1999).
4. A. LOMAX, T. BORTFELD, G. GOITEIN, J. DEBUS, C. DYKSTRA, P. A. TERCIER, P. A. COUCKE, and R. O. MIRIMANOFF, "A Treatment Planning Comparison of Proton and Intensity Modulated Photon Therapy," *Radiother. Oncol.*, **51**, 257 (1999).
5. W. T. CHU, B. A. LUDEWIGT, and T. R. RENNER, "Instrumentation for Treatment of Cancer Using Proton and Light-Ion Beams," *Rev. Sci. Instrum.*, **64**, 2055 (1993).
6. U. SCHNEIDER, S. AGOSTEO, E. PEDRONI, and J. BESSERER, "Secondary Neutron Dose During Proton Therapy Using Spot Scanning," *Int. J. Radiat. Oncol. Biol. Phys.*, **53**, 244 (2002).
7. S. AGOSTEO, C. BIRATTARI, M. CARAVAGGIO, M. SILARI, and G. TOSI, "Secondary Neutron and Photon Dose in Proton Therapy," *Radiother. Oncol.*, **48**, 293 (1998).
8. J. FONTENOT, P. TADDEI, Y. ZHENG, D. MIRKOVIC, T. JORDAN, and W. NEWHAUSER, "Equivalent Dose and Effective Dose from Stray Radiation During Passively Scattered Proton Radiotherapy for Prostate Cancer," *Phys. Med. Biol.*, **53**, 1 (2008).
9. P. J. TADDEI, J. D. FONTENOT, Y. ZHENG, D. MIRKOVIC, A. K. LEE, U. TITT, and W. D. NEWHAUSER, "Reducing Stray Radiation Dose to Patients Receiving Passively Scattered Proton Radiotherapy for Prostate Cancer," *Phys. Med. Biol.*, **53**, 2131 (2008).
10. R. TAYAMA, Y. FUJITA, M. TADOKORO, H. FUJIMAKI, T. SAKAE, and T. TERUNUMA, "Measurement of Neutron Dose Distribution for a Passive Scattering Nozzle at the Proton Medical Research Center (PMRC)," *Nucl. Instrum. Methods A*, **564**, 532 (2006).
11. A. PEREZ-ANDUJAR, W. D. NEWHAUSER, and P. M. DeLUCA, Jr., "Neutron Production from Beam-Modifying Devices in a Modern Double Scattering Proton Therapy Beam Delivery System," *Phys. Med. Biol.*, **54**, 993 (2009).
12. B. GOTTSCHALK, A. KOEHLER, J. SISTERTSON, and M. WAGNER, "The Case for Passive Beam Spreading," *Proc. Proton Radiotherapy Workshop*, Report No. 111, Paul Scherrer Institute (1991).
13. K. MATSUDA, M. UMEZAWA, H. FUJIMAKI, H. NISHIUCHI, M. YANAGISAWA, M. TADOKORO, T. SAKAE, T. TERUNUMA, and Y. AKINE, "Development of Irradiation System with a Range Modulation Wheel and a Contoured Second Scatterer," Progress Report 2000–2005, p. 213, Proton Medical Research Center (2006).
14. W. NEWHAUSER, J. FONTENOT, Y. ZHENG, J. POLF, U. TITT, N. KOCH, X. ZHANG, and R. MOHAN, "Monte Carlo Simulations for Configuring and Testing an Analytical Proton Dose-Calculation Algorithm," *Phys. Med. Biol.*, **52**, 4569 (2007).
15. Y. ZHENG, W. NEWHAUSER, J. FONTENOT, P. TADDEI, and R. MOHAN, "Monte Carlo Study of Neutron Dose Equivalent During Passive Scattering Proton Therapy," *Phys. Med. Biol.*, **52**, 4481 (2007).
16. J. HERAULT, N. IBORRA, B. SERRANO, and P. CHAUVEL, "Monte Carlo Simulations of a Proton Therapy Platform Devoted to Ocular Melanoma," *Med. Phys.*, **32**, 910 (2005).
17. N. KOCH and W. D. NEWHAUSER, "Virtual Commissioning of a Treatment Planning System for Proton Therapy of Ocular Cancers," *Radiat. Prot. Dosim.*, **115**, 159 (2005).
18. J. D. FONTENOT, W. D. NEWHAUSER, and U. TITT, "Design Tools for the Proton Therapy Nozzles Based on the Double-Scattering Foil Technique," *Radiat. Prot. Dosim.*, **116**, 211 (2005).
19. J. C. POLF, M. C. HARVEY, U. TITT, W. D. NEWHAUSER, and A. SMITH, "Initial Beam Size Study for Passive Scatter Proton Therapy. I. Monte Carlo Verification," *Med. Phys.*, **34**, 4213 (2007).

20. U. TITT and W. D. NEWHAUSER, "Neutron Shielding Calculations in a Proton Therapy Facility Based on Monte Carlo Simulations and Analytical Models: Criterion for Selecting the Method of Choice," *Radiat. Prot. Dosim.*, **115**, 144 (2005).
21. U. TITT, Y. ZHENG, O. N. VASSILIEV, and W. D. NEWHAUSER, "Monte Carlo Investigations of Collimator Scatter of Proton-Therapy Beams Produced Using the Passive Scattering Method," *Phys. Med. Biol.*, **53**, 487 (2008).
22. M. F. MOYERS, E. R. BENTON, A. GHEBREMEDHIN, and G. COUTRAKON, "Leakage and Scatter Radiation from a Double Scattering Based Beamline," *Med. Phys.*, **35**, 1, 128 (2008).
23. D. B. E. PELOWIZ, "MCNPX User's Manual Version 2.5.0," LA-CP-05-0369, Los Alamos National Laboratory (2005).
24. H. W. BERTINI, "Low-Energy Intranuclear Cascade Calculation," *Phys. Rev.*, **131**, 1801 (1963).
25. "Nuclear Data for Neutron and Proton Radiotherapy and for Radiation Protection," ICRU Report 63, International Commission on Radiological Units and Measurements (2000).